Drop Size Distribution Retrieval with Polarimetric Radar: Model and Application

EDWARD A. BRANDES, GUIFU ZHANG, AND J. VIVEKANANDAN

National Center for Atmospheric Research, Boulder, Colorado*

(Manuscript received 24 February 2003, in final form 30 September 2003)

ABSTRACT

Polarimetric radar measurements are used to retrieve properties of raindrop distributions. The procedure assumes that drops are represented by a gamma distribution and retrieves the governing parameters from an empirical relation between the distribution shape and slope parameters and measurements of radar reflectivity and differential reflectivity. Retrieved physical characteristics of the drop size distribution (DSD) were generally well matched with disdrometer observations. The method is applied to select storms to demonstrate utility. Broad DSDs were determined for the core (high reflectivity) regions of thunderstorms. Largest drop median volume diameters were at the leading edge of the storm core and were displaced slightly downwind from updrafts. Rainy downdrafts exhibited what are believed to be equilibrium DSDs in which breakup and accretion are roughly in balance. DSDs for stratiform precipitation were dominated by relatively large drops. Median volume diameters at the ground were closely related to the intensity of an overlying bright band. The radar measurements suggest that, although DSDs in stratiform rain were also broad and nearly constant in the rain layer, they were not at equilibrium but were merely steady. DSD invariance is attributed to small total drop numbers, which result in few collisions.

1. Introduction

Dual-polarization radars typically transmit horizontally and vertically polarized electromagnetic waves and receive backscattered signals. Because illuminated hydrometeors are not exactly spherical and are not similarly oriented, wave scattering is different for the two polarizations. Waves propagating through precipitation are subject to scattering, attenuation, phase shifts, and depolarization. Signal properties change continuously as the waves propagate, yielding information regarding particle size, shape, and orientation that can be used to estimate the governing parameters of assumed drop size distribution (DSD) models (Seliga and Bringi 1976; Zhang et al. 2001; Gorgucci et al. 2002; Bringi et al. 2002). A capability to retrieve DSD information would be important for studying precipitation processes and the hydrometeor properties of storms, for validating microphysical parameterizations within numerical models, and for improving rainfall estimates.

Seliga and Bringi (1976, 1978) retrieved two parameters defining an exponential DSD, that is, a concentration parameter and the drop median volume diameter, using measurements of radar reflectivity and differential reflectivity. Subsequent research suggests that, for short time periods commensurate with radar measurements, DSDs are more typically represented by a gamma distribution (Ulbrich 1983),

$$N(D) = N_0 D^{\mu} \exp(-\Lambda D), \tag{1}$$

where N_0 ($\text{mm}^{-\mu-1}\ \text{m}^{-3}$) is a number concentration parameter, μ is a distribution shape parameter, Λ (mm^{-1}) is a slope term, and D (mm) is the drop equivalent volume diameter. Because the gamma DSD is described by three parameters, three measurements or relations are required. The retrieval technique used here, an adaptation of that proposed by Zhang et al. (2001), is based on measurements of radar reflectivity at horizontal polarization (Z_H) and differential reflectivity (Z_{DR}), and an empirical constraining relationship between the drop size distribution shape and slope parameters. The μ–Λ relation was derived from drop size distribution measurements. Concern has been raised as to the influence of measurement errors on such relations (Chandrasekar and Bringi 1987). This issue is addressed by Zhang et al. (2003), who show that the μ–Λ relation is intrinsically different than the linear relation associated with measurement error and that retrieved μ and Λ values are not biased by statistical errors.

Gorgucci et al. (2002) and Bringi et al. (2002) propose to retrieve the DSD from reflectivity, differential reflectivity, and specific differential phase (K_{DP}). The procedure yields the mean axis ratio of the drops, the DSD

* The National Center for Atmospheric Research is sponsored by the National Science Foundation.

Corresponding author address: Dr. Edward A. Brandes, National Center for Atmospheric Research, P.O. Box 3000, Boulder, CO 80307. E-mail: brandes@ncar.ucar.edu

shape factor, a normalized number concentration, and the DSD median volume diameter. There is some question with regard to the use of K_{DP} for DSD parameter retrieval; K_{DP} is computed from measurements of differential propagation phase, which can be noisy, particularly at lower rain rates. To reduce the uncertainty in K_{DP}, the differential phase measurements are filtered in range, often over several kilometers (e.g., Ryzhkov and Zrnić 1996; Hubbert et al. 1993). Retrievals of drop mean shape with K_{DP} can produce large variations in space and time, which have not been independently verified. Further, Illingworth and Blackman (2002) argue that the redundancy among Z_H, Z_{DR}, and K_{DP} precludes the retrieval of the three DSD parameters in Eq. (1) with this parameter set. Rather, K_{DP} is used here for verifying the radar calibration (Vivekanandan et al. 2003). Bringi et al. (2002) apply the method only to situations in which $K_{DP} \geq 0.3^\circ$ km^{-1} (rain rates of greater than 20 mm h^{-1}). Hence, the technique has limited application for general DSD retrieval.

This paper gives an overview of the available data and the DSD retrieval procedure. The method is then applied to moderate thunderstorms, a stratiform rain event, and a strong multicellular thunderstorm. Retrieved total drop concentrations, mass-distribution spectral widths, drop median volume diameters, rainwater content, and rain rates are compared with computations with disdrometer observations and are used to examine the spatial and temporal characteristics of DSDs within the selected storms.

2. Data

Radar measurements used in this study were collected with the National Center for Atmospheric Research's S-band, dual-polarization Doppler radar (S-Pol) in east-central Florida during a special field experiment (''PRECIP98'') to evaluate the potential of polarimetric radar to estimate rainfall (Brandes et al. 2002). Measurements were obtained at high temporal and spatial resolution over a special rain gauge network installed by the National Aeronautics and Space Administration as part of its Tropical Rainfall Measuring Mission. The network included a video disdrometer (Kruger and Krajewski 2002) located 38 km from the radar. One-minute observations were available. Reflectivity and differential reflectivity measurements from the radar were averaged (linear units) over five range gates. Each gate was 0.15 km in length. For comparison with the disdrometer (sections 3 and 4), the smoothed radar measurements for range bins containing the disdrometer and for 0.5° antenna elevation were used. Gridded values of DSD parameters (section 4) were found by averaging retrieved DSD parameters over a volume having a radius of 0.75 km. Proximity to the Weather Surveillance Radar-1988 Doppler (WSR-88D) at Melbourne, Florida, (KMLB) gave dual-Doppler radar coverage over the gauge network and the disdrometer. [For instrument locations see Brandes et al. (2002, their Fig. 1).]

3. DSD parameter retrieval

The method for retrieving the DSD governing parameters follows that of Zhang et al. (2001) as modified by Brandes et al. (2003). The procedure uses the definitions of radar reflectivity and differential reflectivity expressed in terms of the DSD parameters (N_0, μ, and Λ) and drop backscattering amplitudes and an empirical relation between μ and Λ determined from drop observations:

$$\Lambda = 1.935 + 0.735\mu + 0.0365\mu^2. \quad (2)$$

This relation is based upon a representative cross section of storms that included light stratiform to heavy convective precipitation. Drop axis ratios are calculated with

$$r = 0.9951 + 0.025\,10D - 0.036\,44D^2 + 0.005\,030D^3 - 0.000\,249\,2D^4, \quad (3)$$

where r is the axis ratio (vertical axis divided by the horizontal axis). This expression was used by Brandes et al. (2002) for rainfall estimation. Bias factors for polarimetric rainfall estimators using Z_H, K_{DP}, K_{DP} and Z_{DR}, and Z_H and Z_{DR} converged to a similar value, indicating the validity of the relation. The DSD can be found by using the definition of Z_{DR} and the empirical relation [Eq. (2)] to retrieve μ and Λ by iteration and then using the definition of radar reflectivity at horizontal polarization to find N_0.

Once the governing parameters of the DSD are known, other attributes can be computed. The total drop concentration (N_T, m^{-3}) is given by

$$N_T = \int_0^{D_{\max}} N(D)\, dD, \quad (4)$$

where $D_{\max}$, the diameter of the largest drop (mm), is estimated from radar reflectivity (Brandes et al. 2003). The drop median volume diameter (D_0, mm) is defined as

$$\int_0^{D_0} D^3N(D)\, dD = \int_{D_0}^{D_{\max}} D^3N(D)\, dD, \quad (5)$$

and one-half of the rainwater content is contained in drops smaller and one-half in drops larger than D_0. A closely related parameter, the mass-weighted average diameter (D_m, mm), is computed from

$$D_m = \frac{\int_0^{D_{\max}} D^4N(D)\, dD}{\int_0^{D_{\max}} D^3N(D)\, dD}. \quad (6)$$

The variance of the mass spectrum (σ_m^2, mm^2) is given either by (Ulbrich 1983)

$$\sigma_m^2 = \frac{\int_0^{D_{\max}} (D - D_m)^2 D^3 N(D)\, dD}{\int_0^{D_{\max}} D^3 N(D)\, dD} \quad \text{or}$$

$$\sigma_m^2 = (M_5 - 2M_4 D_m + M_3 D_m^2)/M_3, \tag{7}$$

with M_3, M_4, and M_5 being the third, fourth, and fifth moments of the drop size distribution. The rainwater content (W, g m^{-3}) is computed from

$$W = \frac{\rho_w \pi \times 10^{-3}}{6} \int_0^{D_{\max}} N(D) D^3\, dD, \tag{8}$$

and the rainfall rate (R, mm h^{-1}) is computed from

$$R = 6\pi \times 10^{-4} \int_0^{D_{\max}} D^3 v_t(D) N(D)\, dD, \tag{9}$$

where ρ_w is the density of water (g cm^{-3}) and $v_t(D)$ (m s^{-1}), the drop terminal velocity, is computed as in Brandes et al. (2002).

The retrieval method has been previously verified by Zhang et al. (2001) and Brandes et al. (2003). Trends in the integral parameters N_T, D_0, D_m, W, and R are readily retrieved, and biases are generally small. Because N_T (a low moment of the DSD) is derived from radar reflectivity and differential reflectivity (high moments of the DSD), a precise model is required to capture the variance in N_T. Drop concentrations tend to be underestimated with video disdrometers (Tokay et al. 2001). Hence, the estimated drop concentrations from radar and the disdrometer are regarded as approximate. DSD parameters retrieved with the constrained-gamma method are fairly insensitive to variations in $D_{\max}$ and have less bias than retrievals with assumed fixed values of μ. Estimated rain rates have distinct advantages over estimates derived from power-law relations using radar reflectivity or specific differential phase measurements (Brandes et al. 2003). The accuracy of μ and Λ retrievals depends on rain rate. Retrievals and observations are well matched for reflectivity of greater than 30 dBZ (see Brandes et al. 2003, their Fig. 3). Correspondence decreases at light rain rates as the relative error in the radar measurements and statistical variability associated with small disdrometer drop counts increases.

Because of measurement and model error, the above integrals become unreliable for retrieving DSD parameters when $Z_{\rm DR} < 0.3$ dB or $Z_{\rm DR} > 3$ dB. Radar-measured and disdrometer-calculated values of $Z_{\rm DR}$ of greater than 3 dB are occasionally observed at the leading edge of strong convection. Related DSDs typically are characterized by small numbers of very large drops, and calculations with disdrometer observations using the moments method (e.g., Kozu and Nakamura 1991) often yield negative μs. Some of these negative values may arise simply from inadequate sampling of large drop concentrations. Negative μs with the gamma DSD model [Eq. (1)] associate with high concentrations of small drops—not usually observed at the leading edge of strong convection. The constrained-gamma model [Eq. (2)] is designed to match disdrometer observations and will, in general, reproduce the negative μs seen by the disdrometer. However, the retrieval model with integration of drop diameters from 0 mm to $D_{\max}$ may not be applicable in this region of some storms. In this study, $Z_{\rm DR}$ values of greater than 3 dB are ignored. Imposition of an upper limit for $Z_{\rm DR}$ dictates that retrievals in large drop regions, particularly at the leading edge of strong convection, should be viewed skeptically.

For radar measurements with small $Z_{\rm DR}$ (<0.3 dB), a simple set of estimators was derived using the constrained-gamma model. Rain and radar parameters were calculated for Λ in the range of 0.5–13 mm^{-1} and a fixed value of N_0. Ratios of the parameters N_T, W, and R with Z_H are independent of N_0 and are functions of μ (or Λ), determined by $Z_{\rm DR}$ alone for the constrained-gamma DSD. We took logarithms of the ratios and fit them with polynomial functions to obtain

$$N_T = 2.085 Z_H \times 10^{(0.728 Z_{\rm DR}^2 - 2.066 Z_{\rm DR})}, \tag{10}$$

$$W = 5.589 \times 10^{-4} Z_H \times 10^{(0.223 Z_{\rm DR}^2 - 1.124 Z_{\rm DR})}, \quad \text{and} \tag{11}$$

$$R = 0.007\,60 Z_H \times 10^{(0.165 Z_{\rm DR}^2 - 0.897 Z_{\rm DR})}. \tag{12}$$

The units of Z_H and $Z_{\rm DR}$ are linear (mm^6 m^{-3}) and decibels, respectively. Expressions for D_0 and σ_m are functions of $Z_{\rm DR}$ alone and are given by

$$D_0 = 0.171 Z_{\rm DR}^3 - 0.725 Z_{\rm DR}^2 + 1.479 Z_{\rm DR} + 0.717 \quad \text{and} \tag{13}$$

$$\sigma_m = -0.0247 Z_{\rm DR}^2 + 0.519 Z_{\rm DR} + 0.163, \tag{14}$$

with $Z_{\rm DR}$ in decibels. The relations in Eqs. (10)–(14) are unique for the axis ratio relation used and are fundamentally different from that derived from DSD simulations or measurements (e.g., Gorgucci et al. 2002). In general, the integral values [Eqs. (4)–(9)] gave a better match with disdrometer observations. The polynomial relations [Eqs. (10)–(14)] are computationally efficient and provide good estimates of N_T, W, R, D_0, and σ_m for $Z_{\rm DR} \leq 3$ dB. For large $Z_{\rm DR}$, as occasionally seen at the leading edge of strong convection, N_T can be 10^4 m^{-3} (or more). The DSDs for such measurements are dominated by large drops, possibly supported by ice cores, and are probably not well represented by the constrained-gamma model.

A retrieval for the standard deviation (width) of the mass spectrum σ_m, not shown previously, is presented in Fig. 1. Spectrum widths for the disdrometer observations were computed from the DSD moments; radar-based widths were computed from the polynomial relation in Eq. (14). The radar-retrieved values tend to be a little smaller on average than that computed for the disdrometer measurements (<0.1 mm). However, it is

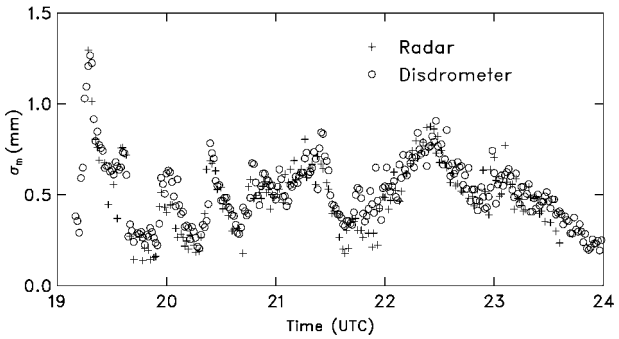

FIG. 1. Drop distribution spectral width (σ_m) as retrieved by radar and computed from disdrometer measurements for a series of storms on 17 Sep 1998.

clear that the constrained-gamma method provides useful detailed information about DSDs.

The method for retrieving DSD parameters makes use of known raindrop characteristics and shapes and is not applicable to solid (frozen) precipitation. Hence, retrievals are reproduced only for storm levels well below the melting level. Hail and nonmeteorological targets, such as insects and ground clutter, may contaminate the radar measurements and adversely influence the retrievals. To minimize contamination, we adapted the procedure of Aydin et al. (1986). Radar reflectivity and differential reflectivity, computed for video disdrometer observations collected during PRECIP98, regardless of rain rate and drop counts, are plotted in Fig. 2. The region between the curves is thought to represent ''good'' data points. Note that the upper curve excludes a small number of data points for reflectivities of less than 35 dBZ. These points are all characterized by small sample sizes ($N_T < 200$ m^{-3}) and are dominated by large drops that, in general, are poorly sampled with disdrometers because of the small sample volume. Radar measurements of Z_H and Z_{DR} closely agreed with disdrometer observations (Brandes et al. 2002); hence, the two curves were used to ''edit'' the radar measurements. Only measurements between the curves were accepted for analysis. Hail increases radar reflectivity, and a tendency to tumble while falling reduces the differential reflectivity relative to the rain-only case. Measurements contaminated by large hail lie to the right of the lower curve in Fig. 2—generally in the region with reflectivity >40 dBZ. Displacement from the curve increases as hail size increases (Aydin et al. 1986; Brandes and Vivekanandan 1998). At low reflectivity, statistical errors in the Z_{DR} measurement and ground targets can result in data points below the lower curve. When applied to radar data, the upper boundary eliminates some measurements that are dominated by unusual distributions of large drops. The boundary also eliminates measurements strongly influenced by nonmeteorological factors such as ground returns and insects.

The sharp edge of data points at the lower boundary in Fig. 2 is a common feature of calculations with ob-

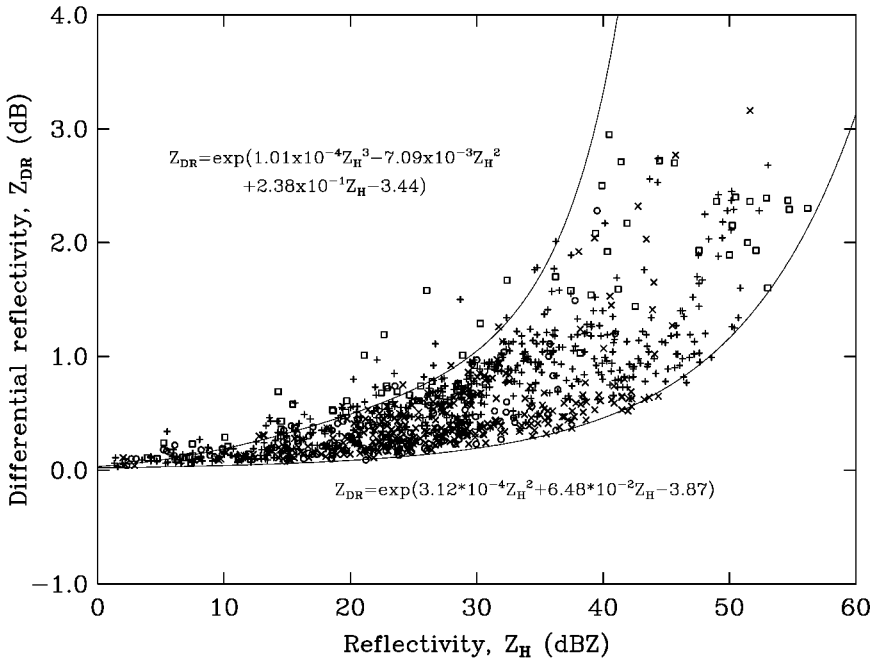

FIG. 2. Radar reflectivity plotted against differential reflectivity as computed from disdrometer observations. The curved lines delineate observations with drop counts ≥200 and are used to discriminate radar measurements contaminated by nonmeteorological targets and hail from ''rain only'' measurements. DSD shape parameter values are indicated (□: $\mu < 0$; +: $0 \le \mu < 4$; ×: $4 \le \mu < 8$; ○: $\mu > 8$).

served drop size distributions and radar measurements. There is a tendency, in particular at moderate reflectivity values, for the shape parameters of the DSDs in Fig. 2 to increase from left to right. Thus, for a particular Z_{DR} value, the DSD narrows (becomes less exponential) as the reflectivity (along with rain intensity) increases. For a specified Z_H value, there is also a tendency for μ, Λ, and R to increase toward the lower boundary. The latter data points are predominantly convective. DSDs at the lower boundary are somewhat narrower and have greater slopes for the large drop portion of the distribution than those at the upper boundary. Moreover, they have the minimum drop median volume diameters, the highest total drop concentrations, and highest rain rates for a particular reflectivity value. In converse, DSDs near the upper boundary have the largest median volume diameters for a specified reflectivity. This boundary, as the plotted data suggest, is less defined because of the sampling issues associated with small concentrations of large drops.

Hu and Srivastava (1995) studied drop breakup and accretion effects on simulated DSDs. They found that, regardless of the initial distribution, essentially parallel equilibrium DSDs in which drop breakup and accretion were balanced evolved over periods of 10 min and falls of 2 km. Hence, equilibrium DSDs are believed to be manifest by constant values of μ and Λ (Sauvageot and Lacaux 1995; Atlas and Ulbrich 2000). With our retrieval model, constant Z_{DR} is an indication of constant μ and Λ. Hu and Srivastava determined that the time required for an equilibrium distribution to form was inversely proportional to the rain rate. DSDs at the lower boundary in Fig. 2 are believed to be near equilibrium and not quite exponential. They may bear little resemblance to their initial distribution upon melting. In contrast, data points near the upper boundary represent DSDs dominated by large drops and relatively low rain rates and drop numbers. Hence, these DSDs are believed to evolve more slowly and to retain more of their initial characteristics.

4. DSD retrieval examples

In this section, the DSD retrieval method is applied to several storm types. Results are compared with disdrometer observations to verify the utility of the retrievals. Also, the spatial and temporal distributions of the retrieved fields are examined for consistency with storm kinematics.

a. Moderate thunderstorms

During the late morning hours on 21 August 1998 two short east–west lines or bands of moderate thunderstorms developed in east-central Florida (Fig. 3a). The convection drifted toward the west-southwest. The southernmost line passed over the disdrometer. A comparison of radar reflectivity and differential reflectivity, as measured by radar and computed from disdrometer observations, is shown in Figs. 4a,b. Although there was a separation of 38 km between the instruments, the radar sampling volume is many orders of magnitude larger than that of the disdrometer, and the radar beam was 400 m above the disdrometer, the agreement is good. There are significant differences. Some disdrometer-based radar reflectivities associated with the leading convection are 3–8 dB higher than that measured by radar. At 1515 UTC, a transition period between convective and stratiform rainfall, the disdrometer reflectivities fall below 10 dB*Z* while the radar-measured values remain larger than 17 dB*Z*. For the more stratiform component of the precipitation (1520–1600 UTC), the range of extreme values in the wavelike reflectivity trace are slightly wider with the disdrometer. A similar relationship can be seen with differential reflectivity. The suppressed maxima and raised minima in the radar measurements are attributed to greater smoothing with the larger radar measurement volume. A mean (calibration) bias is not evident.

Figures 4c,d show the comparison for total drop concentration and for median volume diameter using the procedure described in section 3. Trends are well matched. On average, radar-derived drop concentrations are smaller. The difference is most noticeable for the period of stratiform rainfall. It is possible that the discrepancy lies with retrieving the zero-order moment of the DSD from higher-order measurements, that the rain-observed DSDs may not be described well by the constrained-gamma distribution, or that there is significant advection of precipitation below the elevated radar beam. Differences in N_T are not necessarily transferred to W, R, D_0, D_m, and σ_m, because these parameters have higher correlation with Z_H and Z_{DR}. Note that a significant mean bias is not evident in the retrieved D_0s. Reflectivity and differential reflectivity measurement pairs during the period of stratiform rain vary between 20 dB*Z* and 0.4 dB and 32 dB*Z* and approximately 1 dB. If these measurements were plotted on Fig. 2, they would be near the upper boundary, suggesting that the DSDs were dominated by relatively large drops.

A dual-Doppler wind field analysis (storm relative) is presented in Fig. 5. At 0.5 km (Fig. 5a) the prevailing flow is from the storm's left rear (east-southeast). Note that the disdrometer site is in a reflectivity gradient region on the north side of the southernmost convective band. Advection of precipitation, particularly small drops, below the radar beam could have caused the higher drop concentrations detected by the disdrometer.

Low-level vertical velocities in the convective bands are predominantly downdrafts as suggested by the general acceleration of the horizontal wind from east to west. With height the updrafts became widespread. Winds throughout much of the southern band veer (become more southerly) with height between 0.5 and 2 km (Fig. 5b). In contrast, the northern convective band exhibits strong northeasterly flow at 2 km. This flow

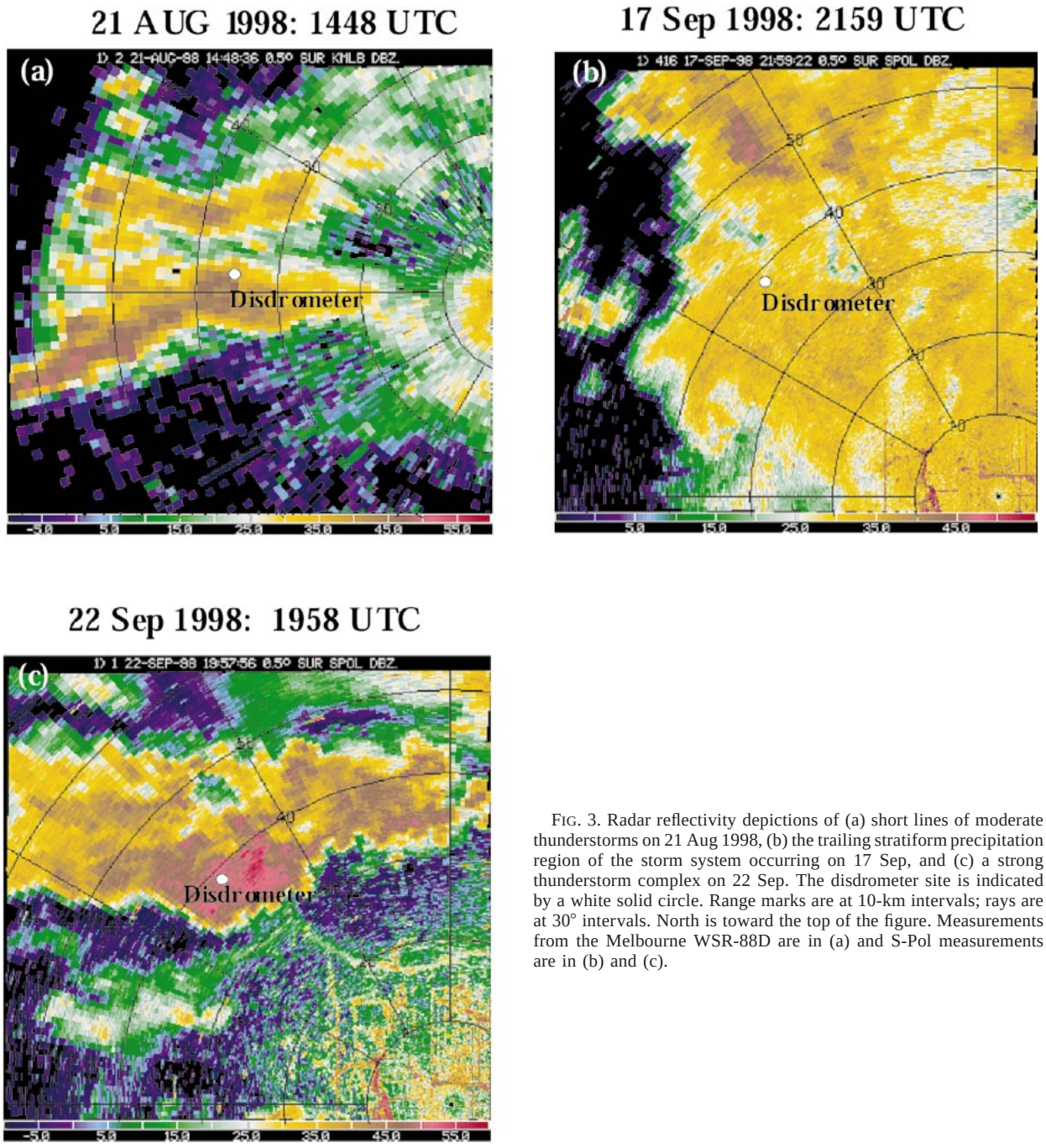

FIG. 3. Radar reflectivity depictions of (a) short lines of moderate thunderstorms on 21 Aug 1998, (b) the trailing stratiform precipitation region of the storm system occurring on 17 Sep, and (c) a strong thunderstorm complex on 22 Sep. The disdrometer site is indicated by a white solid circle. Range marks are at 10-km intervals; rays are at 30° intervals. North is toward the top of the figure. Measurements from the Melbourne WSR-88D are in (a) and S-Pol measurements are in (b) and (c).

overtakes the southern band at 4 km (not shown) and helps to sustain the elevated updrafts. Reflectivity maxima in the southern band slope southward with height; those in the northern band slope eastward.

Physical DSD parameters at 0.5 km are presented in Fig. 6. Inspection reveals that peak drop concentrations in the southern convective line are 3000–5000 m^{-3}. Maximum concentrations in the northern line are about 3000 m^{-3}. Concentrations at the edges of the bands are $<$300 m^{-3}. Estimated drop median volume diameters in the core of the southern convective band (the region with reflectivity $>$40 dBZ) are fairly uniform between 1.4 and 1.8 mm. The region with $D_0 > 1.6$ mm is displaced slightly from the region with reflectivity $>$40 dBZ. This result could be a size-sorting effect in which large drops are the first to fall from the elevated storm core.

Rainwater contents with the southern convective band are mostly 0.5–3 g m^{-3}, and rainfall rates are all $<$60 mm h^{-1}. Somewhat smaller values characterize the

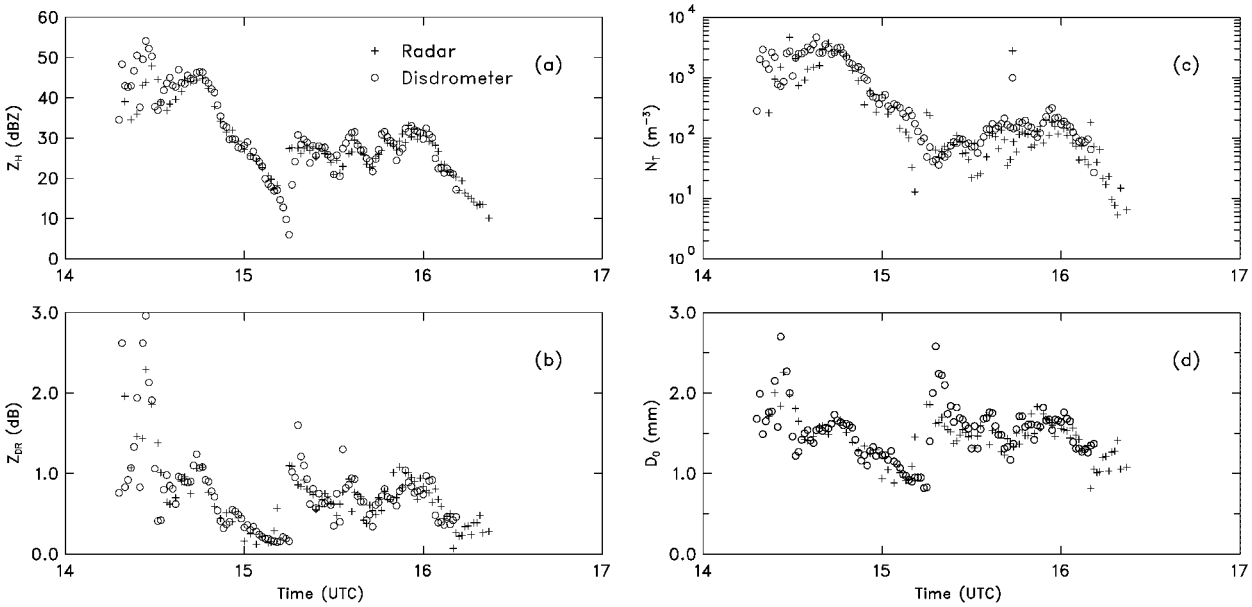

FIG. 4. Radar–disdrometer time plots of (a) radar reflectivity (Z_H), (b) differential reflectivity (Z_{DR}), (c) total drop concentration (N_T), and (d) drop median volume diameter (D_0). The radar antenna elevation is 0.5°.

northern band. An interesting feature of the southern band is that the 1 g m^{-3} rainwater content contour nearly coincides with the 40-dBZ contour. This relation is also true for the 20 mm h^{-1} rain-rate contour. This relationship is altered slightly in the northern band. The correspondence is an indication of reduced dependence on differential reflectivity in this case. Correlations between rainwater content and rain rate with radar reflectivity have long been exploited through the use of power-law relations.

b. Stratiform rain

On 17 September, a line of thundershowers moved from west to east across central Florida. As the line approached the east coast, a large region of stratiform

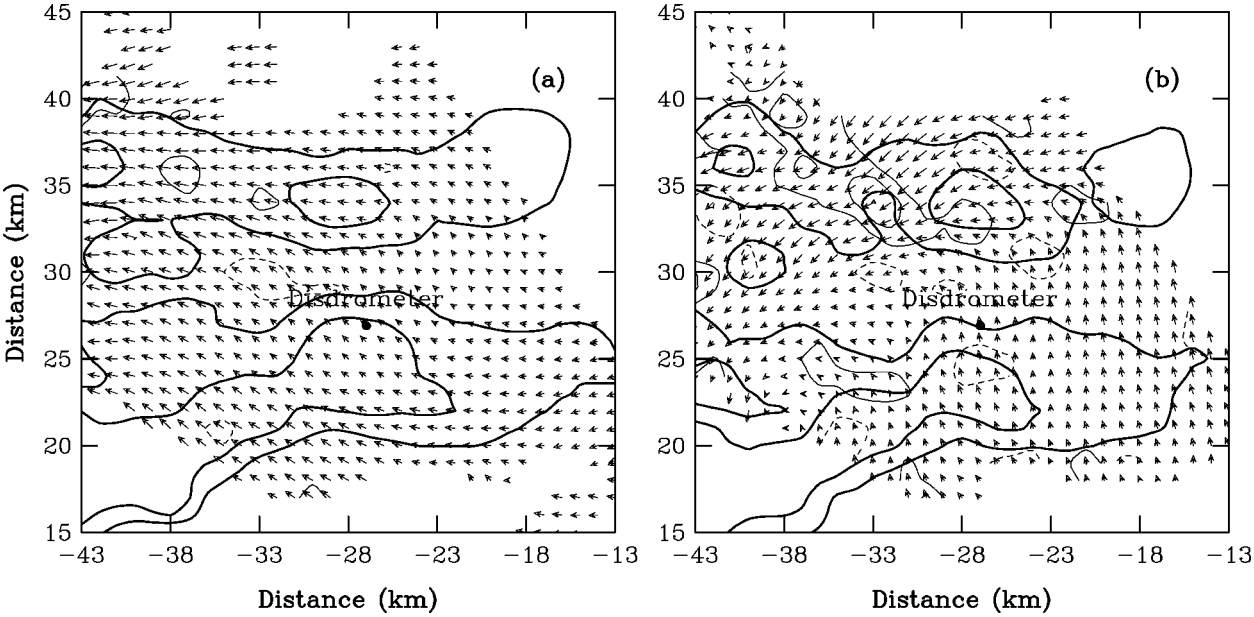

FIG. 5. Storm-relative, dual-Doppler wind field analyses at (a) 0.5- and (b) 2-km height for the thunderstorms of 21 Aug (1448 UTC). Melbourne WSR-88D reflectivity contours for 30 and 40 dBZ are shown (heavy solid contours). Thin solid (dashed) contours show updrafts (downdrafts) ≥0.5 m s^{-1} at 0.5 km. The velocity contour interval is 1 m s^{-1} at 2 km. North is toward the top of the figure.

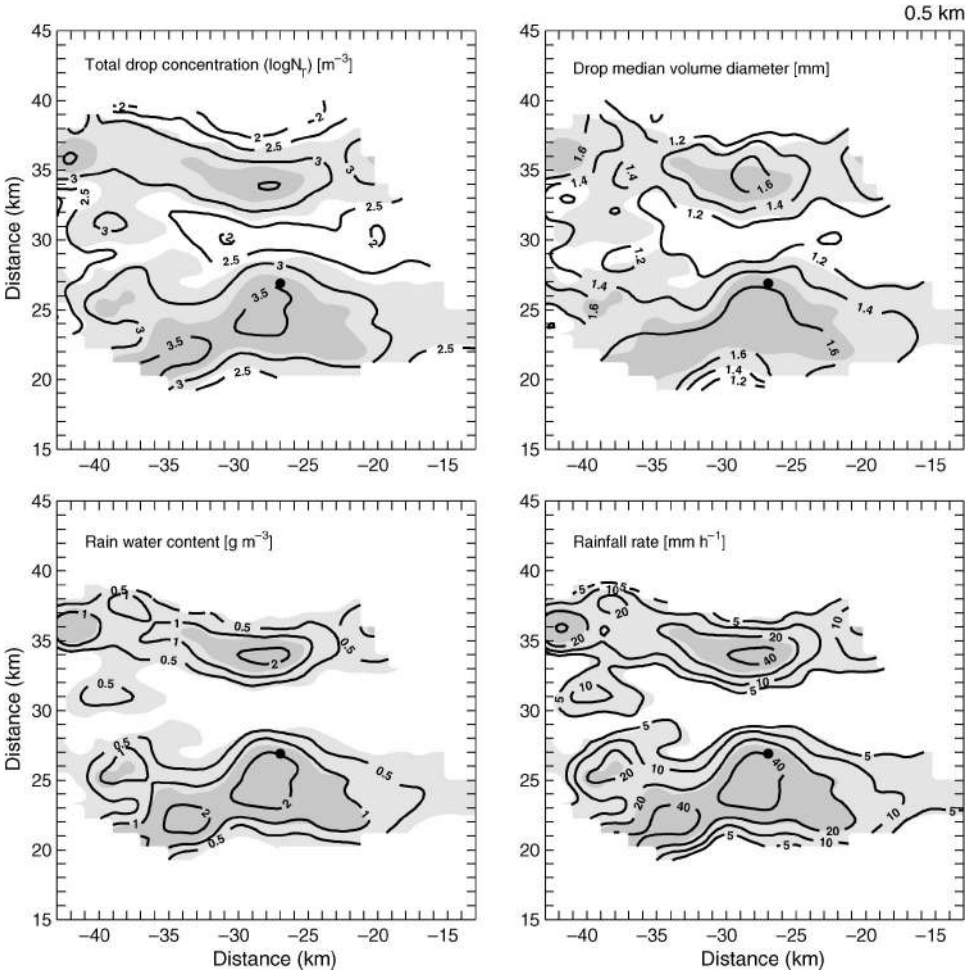

FIG. 6. Retrieved total drop concentration, median volume diameter, rainwater content, and rain rate at 0.5 km for the 21 Aug thunderstorms (1448 UTC). Light shading shows radar reflectivity ≥30 dBZ, as measured with the S-Pol radar; dark shading shows reflectivity ≥40 dBZ. The disdrometer site is shown by a dot.

precipitation with embedded moderate convection formed in its wake (Fig. 3b). Stratiform precipitation, which drifted northward over the disdrometer site, was particularly uniform. A radar-reflectivity bright band associated with the melting layer first appeared over the disdrometer site at 2135 UTC. Maximum brightband reflectivity in the column above the disdrometer is shown in Fig. 7a. Brightband intensity increased to a peak value of 46 dBZ at 2212 UTC. Reflectivity in the column then waned until a second wave of less-intense precipitation moved over the site. Peak brightband reflectivity with this wave was 37 dBZ—measured at 2258 UTC. Profiles of radar reflectivity and differential reflectivity at the time of the two maxima are presented in Fig. 8. (The 0°C level as determined from a 2200 UTC sounding released at the Kennedy Space Center was 4.99 km.)

Figure 7b shows drop median volume diameters as computed from disdrometer observations and estimated from radar measurements. Although the radar-derived D_0s are a little smaller than their disdrometer counterparts (~0.1 mm), the overall agreement is excellent.

The reflectivity bright band associates with large, partly melted particles whose precise structure and composition are not known. However, the large increase in reflectivity of 12–13 dB between the break in the reflectivity lapse (~5 km) and the brightband maximum is suggestive of large aggregates rather than convective debris or graupel (see Klaassen 1988). Regardless, Fig. 7 reveals a close relationship between brightband intensity and the size of drops deposited at the surface. This relationship was examined by Huggel et al. (1996) who determined that well-defined bright bands were an indicator of broad drop distributions with comparatively high concentrations of large drops. A similar relation holds here.

Examination of the radar profiles (Fig. 8) discloses little change in either radar reflectivity or differential

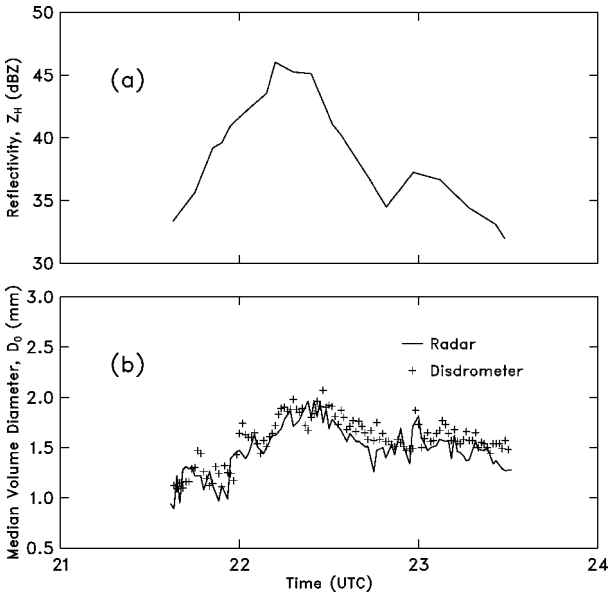

FIG. 7. (a) Maximum brightband reflectivity at the disdrometer site for the stratiform rainfall event of 17 Sep. (b) The median drop diameter as estimated from disdrometer observations and radar measurements.

reflectivity in the rain layer below 3 km. If drop growth by accretion were the dominant process in the layer, reflectivity and differential reflectivity would increase toward the ground. If large drop breakup was the dominant process, reflectivity and differential reflectivity would decrease toward ground.

Rain-layer radar measurements at the disdrometer site (Fig. 8) show an average reflectivity of about 35 dB*Z* and a differential reflectivity of 1 dB at 2212 UTC and a reflectivity of 29 dB*Z* and a differential reflectivity of 0.6 dB at 2258 UTC. These measurements are close to the upper boundary in Fig. 2. Associated median volume diameters computed for the rain layer are 1.65 and 1.46 mm. DSD shape factors, as calculated from disdrometer measurements and retrieved from radar measurements, are roughly 0–2 and 2–4 for the heavier rainfall in the two waves. Hence, the distributions are broad, particularly for the earlier period when the bright band is strongest. The constancy of the radar measurements suggests that DSDs resulting from melted snowflakes are little altered over the lowest 3 km. Rain rates calculated from the disdrometer measurements are at most 11 mm h^{-1} and are typically much less. The Hu and Srivastava (1995) study suggests that at these rates an equilibrium DSD, in which drop breakup and accretion are in balance, would evolve slowly. Hence, the observed distributions, although broad and steady, are likely dominated by the large drops created by aggregation and have not achieved the equilibrium conditions of DSDs at the lower boundary in Fig. 2.

Retrieved spatial distributions of N_T, D_0, W, and R at 2212 UTC are presented in Fig. 9 for a height of 0.5 km. Except for the western edge of the rainfall shield and for a moderate embedded convective cell near the northern edge of the domain ($x = -30$, $y = 43$ km), parameter gradients are small. Where reflectivity exceeded 35 dB*Z*, retrieved drop concentrations are generally 300–600 m^{-3}. Median volume diameters vary from 1.6 to 1.9 mm. Retrieved rainwater contents are mostly less than 0.3 g m^{-3}, and rain rates roughly vary from 4 to 8 mm h^{-1}. Minute-to-minute drop counts at

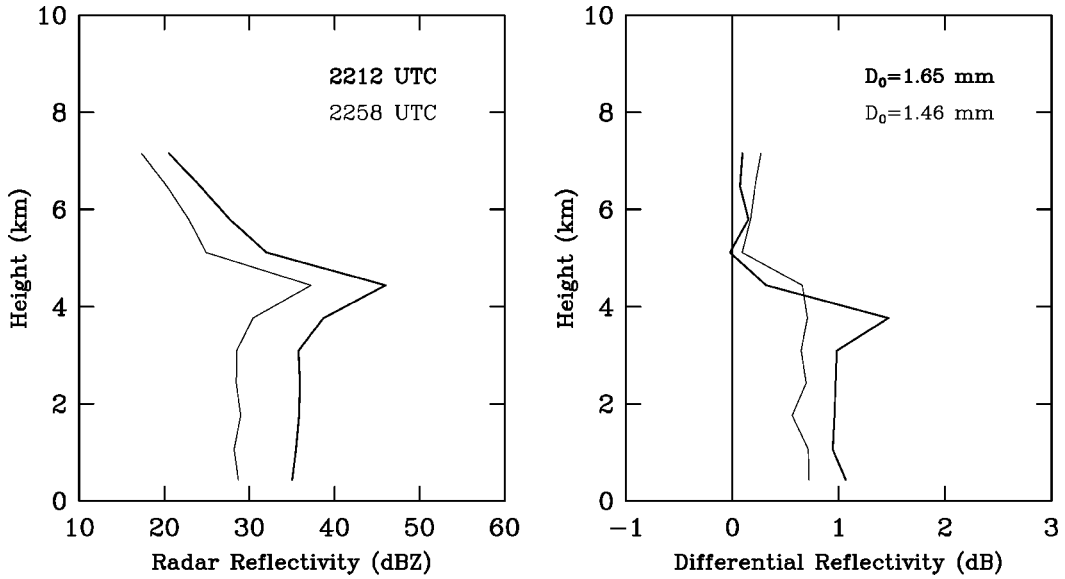

FIG. 8. Profiles of radar reflectivity and differential reflectivity, as measured by radar at 2212 and 2258 UTC for the stratiform event of 17 Sep. Median volume drop diameters (D_0) for the rain layer (surface–3 km), computed from the integral relations, are also shown.

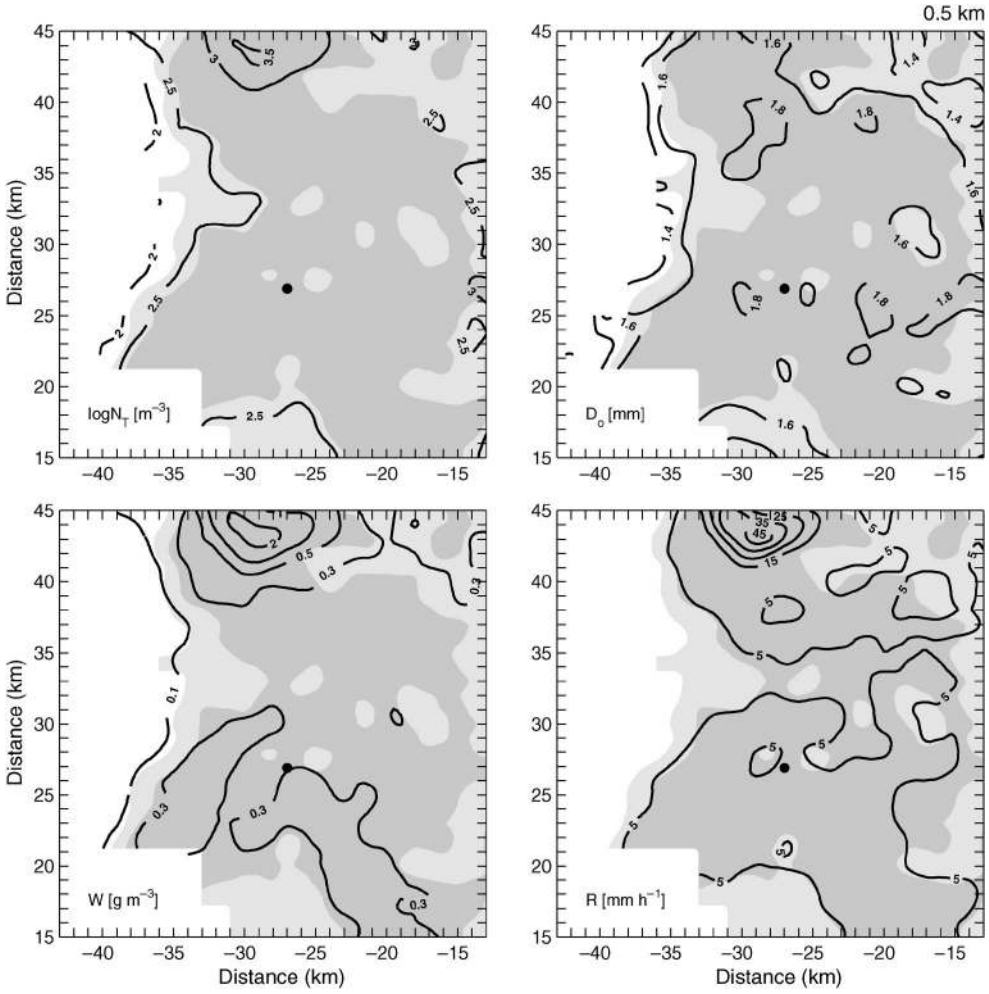

FIG. 9. Retrieved drop size distribution parameters and disdrometer site as in Fig. 6 but for the stratiform region of the 17 Sep event (2209 UTC). Light shading shows radar reflectivity ≥30 dBZ, as measured with the S-Pol radar; dark shading shows reflectivity ≥35 dBZ.

the disdrometer site varied from 399 to 517 m^{-3} between 2209 and 2215 UTC. During this period, median volume diameters were 1.40–1.88 mm, rainwater contents were 0.21–0.28 g m^{-3}, and rain rates were 4.4–6.4 mm h^{-1}.

c. Strong thunderstorm complex

Figure 10 shows a storm-relative, dual-Doppler wind field analysis at 1956 UTC for a strong thunderstorm complex that developed on 22 September. The complex was part of a larger area of showers that propagated toward the east (Fig. 3c). Individual convective cells formed in the updraft and reflectivity gradient region at the storm's leading edge [between $x = -28$, $y = 20$ km and $x = -15$, $y = 30$ km (0.5 km, Fig. 10a)] and moved northwestward through the complex. New cells formed in response to convergence between low-level outflow that originated in weak downdrafts along the storm's northern edge and in a somewhat stronger rainy downdraft within the westward extension of the precipitation core ($x = -32$, $y = 26$ km) and the ambient wind. The latter flow can be seen entering the storm at 2 km (Fig. 10b). That the south-to-southeasterly flow is the primary updraft source is confirmed by the conservation of momentum at higher levels in the updraft (Figs. 10c,d).

At mid- and upper storm levels (e.g., 6 km) hydrometeors growing and lifted in updrafts were carried toward the storm's rear (northwest) and western portions of the precipitation core. Size sorting undoubtedly occurred as particles passed through the updraft. The largest particles would have fallen first, remaining near the updraft core, and lighter particles would have been carried farther to the storm's rear. Frozen particles lifted in updrafts would eventually have fallen within downdrafts and weaker updrafts in the storm's northern and western quadrants. Hydrometeors with sufficient terminal velocities and size to prevent their evaporation would have fallen to lower levels and been borne by the wind back toward the front of the storm complex.

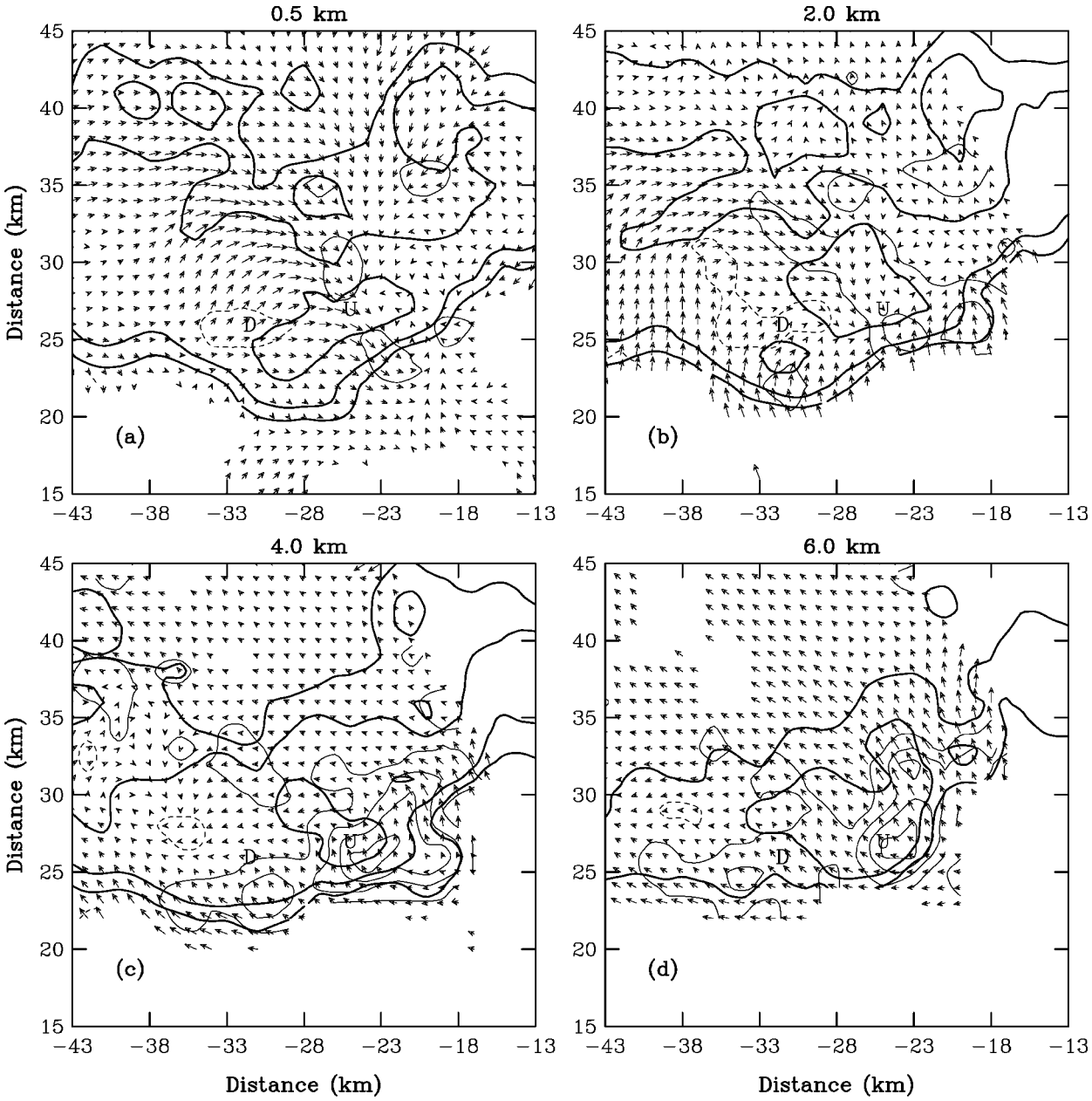

FIG. 10. Wind field analyses as in Fig. 5 but at 1956 UTC for the thunderstorm complex of 22 Sep. Reflectivity contours beginning at 30 dB*Z* and at 10 dB intervals, as measured with the Melbourne WSR-88D, are shown. Thin solid (dashed) contours show updrafts (downdrafts). Contour intervals are 1 m s^{-1} at 0.5 km and 2 m s^{-1} at and above 2 km. The location of measurement profiles for downdraft (D) and updraft (U) regions, as in Fig. 13, are indicated.

Figure 11 presents retrieved DSD physical parameters for 1956 UTC. Inspection reveals that high total drop concentrations coincide with the storm core, that is, the region with radar reflectivity roughly ≥50 dB*Z*. Concentrations greater than 10 000 m^{-3} are indicated. A peak value, on the order of 32 000 m^{-3}, corresponds with a newer convective cell near the leading edge of the storm core ($x = -25$, $y = 27$ km). In truth, the concentrations for this cell seem too high. (Video disdrometer data are not available for this event.) Some Z_{DR} measurements at the leading edge of the storm core were nearly 4 dB. The implication is that huge drops, perhaps supported by ice cores, were present. The extreme Z_{DR}s exceed the limits of the data used to develop the constrained-gamma model (Fig. 2). Moreover, associated DSDs may be poorly described by the constrained-gamma model. Note also that exclusion of Z_{DR} measurements >3 dB from the analysis will cause underestimates of D_0, *W*, and *R*. Retrievals for two older storm cells (near $x = -32$, $y = 32$ km and $x = -27$,

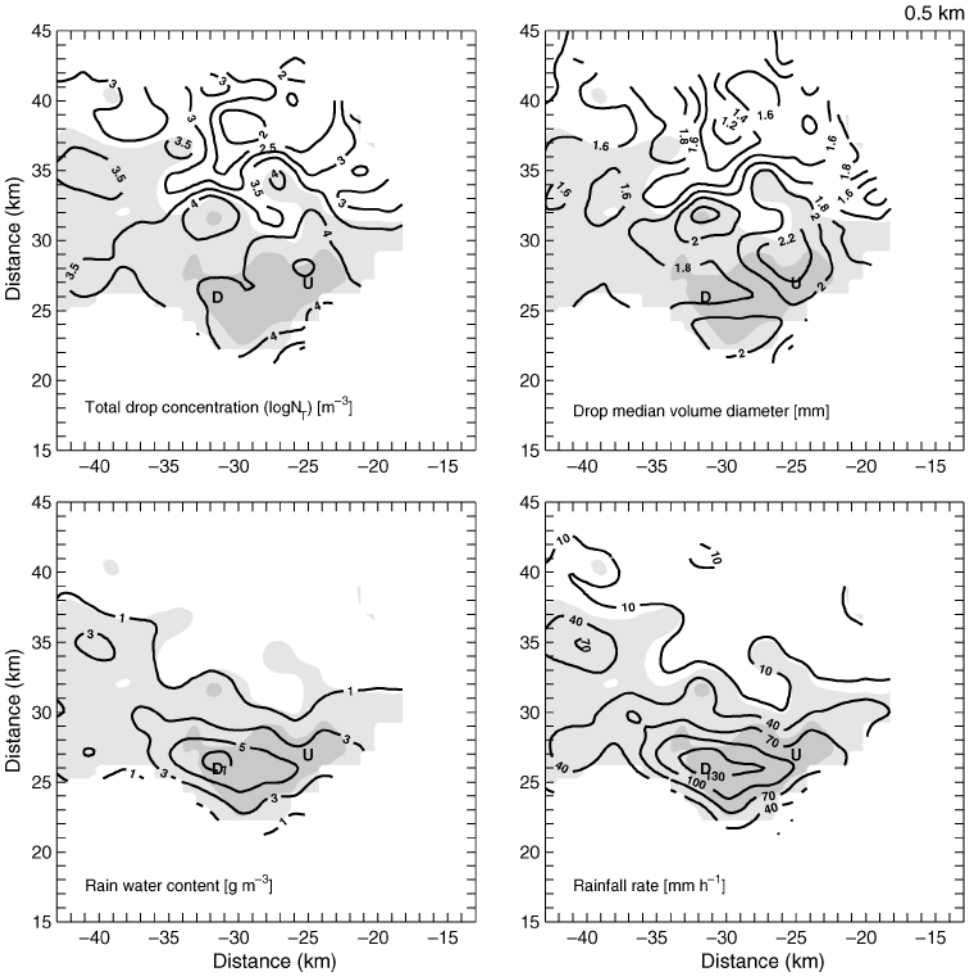

FIG. 11. Retrieved drop size distribution parameters as in Fig. 6 but at 1956 UTC for the 22 Sep thunderstorm. Light shading shows reflectivity ≥40 dBZ, as measured with the S-Pol radar; dark shading shows reflectivity ≥50 dBZ. The locations of measurement profiles for downdraft (D) and updraft (U) regions in Fig. 13 are indicated.

y = 34 km) with relatively high drop concentrations and large drop median volume diameters are believed to be plausible.

The distribution of large D_0s seems dictated, for the most part, by the configuration of updrafts and advection by the horizontal wind. Centers of large D_0 are displaced downwind relative to the updraft. Drop concentrations and D_0s at the rear of the storm complex fall below 100 m^{-3} and 1.4 mm, respectively. The maximum retrieved rainwater content is 7.6 g m^{-3}. This extreme value resides in the trailing portions of the storm core where radar reflectivity is high (>50 dBZ), total drop concentrations are large (>10 000 m^{-3}), and drop median volume diameters are relatively small (<1.8 mm). Peak rainwater content and rain rate (~150 mm h^{-1}) at 0.5 km roughly coincide with the rainy downdraft. Unlike the moderate convective case discussed earlier, there is much crossing of the reflectivity contours by the rainwater content and rain-rate contours. Rainwater contents along the 50-dBZ contour vary from 3 to 7 g m^{-3}, and rain rates vary from 70 to 130 mm h^{-1}. The variation in the retrieved parameters comes from the differential reflectivity measurements and illustrates potential problems with rain-rate algorithms based on reflectivity alone.

Examination of the retrieved DSD shape parameters (Fig. 12) indicates that the DSD is broad within the storm core. Broadening is implied by small values of μ. In fact, there is a large region of slightly negative μs. This result could be due to retrieval model error, but, as noted earlier, the model is merely reproducing characteristics of the disdrometer observations. In general, the negatives are believed. However, at the leading edge of the storm core, aforementioned issues regarding large drops and related concentrations of small drops may come into play. Although small μ values exist in spots along the northern edge of the storm, in general, DSDs at the edge of the storm, where rain rates are

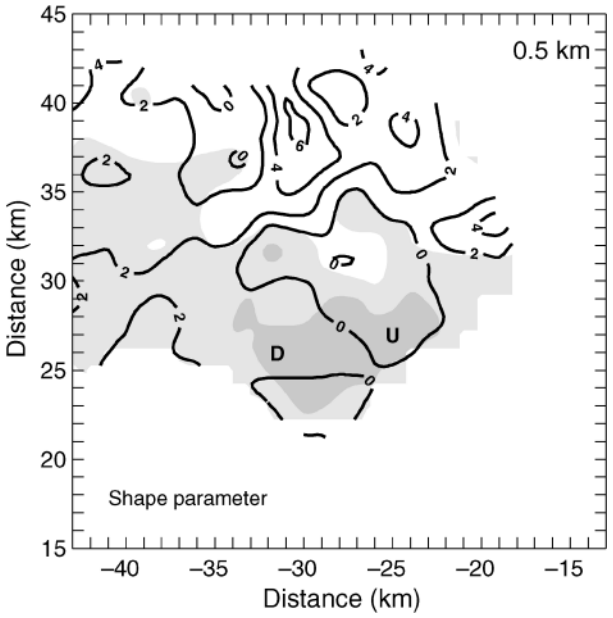

FIG. 12. Retrieved DSD shape parameter at 1956 UTC for the 22 Sep thunderstorm. Reflectivity and profile locations are as in Fig. 11.

light, tend to be more peaked, with typical μ values of 2–6.

Figure 13 displays radar reflectivity and differential reflectivity profiles within the updraft region and the rainy downdraft. The updraft profile shows peak low-level reflectivity of more than 50 dBZ and differential reflectivities that exceed 2 dB. Reflectivity in the rainy downdraft is about 4 dB less, but the differential reflectivity is much lower. The retrieved DSD shape is concave upward ($\mu = -1.0$) for the updraft profile and is slightly positive ($\mu = 1.4$) for the rainy downdraft. A simple interpretation is difficult because of the three-dimensional nature of the storm flow and the rapidity at which the convective elements evolve. However, the downdraft region with a higher rain rate, smaller D_0, and slightly peaked DSD would seem to be closer to an equilibrium distribution than the updraft region.

5. Summary and conclusions

A method for retrieving the governing parameters of gamma DSDs from remote polarimetric radar measurements was applied to subtropical rainfall events. The method utilizes radar reflectivity and differential reflectivity measurements and an empirical relation between the DSD shape and slope parameters. The constraining μ–Λ relation was derived previously from disdrometer observations. Overall, good agreement was found between retrieved DSD parameters and disdrometer observations for a moderate thunderstorm and a stratiform rain event. Retrievals for a strong convective system seemed reasonable except at the leading edge of the convective core where total drop concentrations may have been overestimated. The problem was ascribed to peculiar DSDs with unusual large drop concentrations that are not well represented by the constrained-gamma model.

DSD retrievals for the stratiform event near its peak intensity revealed total drop concentrations on the order of 300–600 m^{-3}, median volume diameters of 1.6–1.9 mm, rainwater contents of 0.3 g m^{-3}, and rain rates of 4–8 mm h^{-1}. The retrievals were in good quantitative agreement with disdrometer measurements. It was found

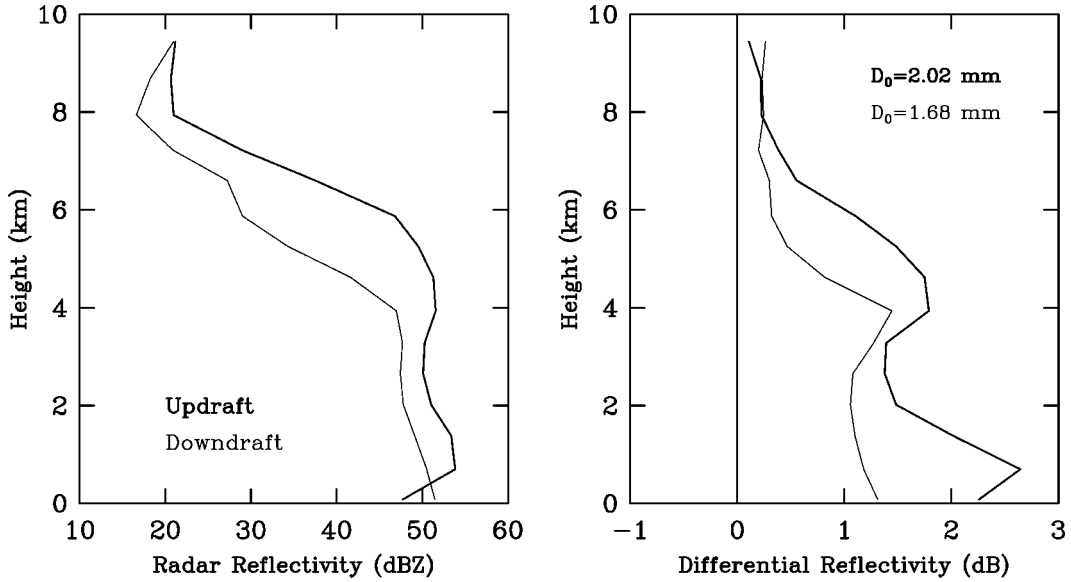

FIG. 13. Profiles of radar reflectivity and differential reflectivity and drop median volume diameter as in Fig. 8 but at 1956 UTC for the 22 Sep thunderstorm. Profiles are for updraft and downdraft regions (see Fig. 10).

that drop D_0s at the ground were highly correlated with the strength of the overlying radar-reflectivity bright band. As the intensity of the bright band increased from less than 35 to more than 45 dBZ, D_0s increased from 1 to 1.8 mm. Precipitation near the ground was characterized by relatively broad DSDs with small values (0–4) of the shape parameter. Reflectivity and differential reflectivity were constant in the rain layer. Observed rain rates were light (generally <10 mm h^{-1}), drop median volume diameters were large (1.4–1.9 mm), and total drop concentrations were low (<600 m^{-3}). Although the stratiform rain DSDs were broad and constant with height, an equilibrium distribution, in which drop coalescence and breakup are roughly in balance, may not have had sufficient time to evolve.

Total drop concentrations in excess of 10 000–30 000 m^{-3} were determined in the core region of a strong convective storm (defined as the region with reflectivity $\geq$50 dBZ). Highest concentrations were in leading portions of the core where updrafts prevailed. This region was characterized by some of the largest retrieved median volume diameters (2.0–2.4 mm). Retrieved DSD shape factors along leading portions of the storm core had negative values, which imply large numbers of small drops with the gamma DSD model. Some disdrometer-derived negatives are undoubtedly real; others may arise simply from inadequate sampling of large drop populations. Although the leading edges of some storms are characterized by large drops, the DSDs do not necessarily have the concentration of small drops inferred by the gamma model. In these cases and wherever significant size sorting occurs, the constrained-gamma model may not apply. The constrained-gamma retrieval model, in general, reproduces the observed negative μs; however, because error in the retrieval propagates in a manner similar to that in the moment fitting of observed DSDs, the retrieved N_T with integration of drops from 0 mm to $D_{\max}$ may be a poor representation of the total drop concentration at the leading edge of some convective storms and should be viewed cautiously. Retrievals for W, R, D_0, D_m, and σ_m should be more reliable.

Maximum rainwater contents of nearly 8 g m^{-3} and rain rates of 150 mm h^{-1} were retrieved in trailing regions of the storm core where a rainy downdraft resided. The downdraft was characterized by high reflectivity, relatively low differential reflectivity, and relatively small drops. DSDs in the rainy downdraft were characteristic of DSDs thought to be close to equilibrium, that is, having upper limits of drop number counts and rain rate as well as minimum D_0 for a particular reflectivity measurement. Shape parameter values generally increased toward the lateral boundaries of the storm complex, signifying that DSDs in these regions were more monodispersed.

Additional radar–disdrometer comparisons are clearly needed—preferably at short distances to minimize sampling differences. Further improvement in the retrieval method may be possible. The differential propagation phase measurement is not used in the retrieval method examined here. The parameter is sensitive to the total rain content and drop shape and is insensitive to attenuation, and it potentially could be used as an additional constraint to reduce bias. Also, the issue of drop concentrations at the leading edges of convective cells needs further investigation. Nevertheless, this study demonstrates that useful DSD information can be deduced from polarimetric radar measurements.

Acknowledgments. The authors are grateful to Drs. Anton Kruger and Witold Krajewski of The University of Iowa for providing the video disdrometer data. Benjamin Hendrickson and Kyoko Ikeda of the National Center for Atmospheric Research (NCAR) helped with data analysis and the construction of the figures. The assistance of the NCAR Atmospheric Technology Division staff throughout the PRECIP98 field program and the analysis phase of this study is gratefully appreciated. This research was supported by funds from the National Science Foundation designated for the U.S. Weather Research Program at NCAR.

REFERENCES

Atlas, D., and C. W. Ulbrich, 2000: An observationally based conceptual model of warm oceanic convective rain in the Tropics. *J. Appl. Meteor.*, **39,** 2165–2181.

Aydin, K., T. A. Seliga, and V. Balaji, 1986: Remote sensing of hail with a dual-linear polarization radar. *J. Climate Appl. Meteor.*, **25,** 1475–1484.

Brandes, E. A., and J. Vivekanandan, 1998: An exploratory study in hail detection with polarimetric radar. Preprints, *14th Int. Conf. on Interactive Information and Processing Systems for Meteorology, Oceanography, and Hydrology*, Phoenix, AZ, Amer. Meteor. Soc., 287–290.

——, G. Zhang, and J. Vivekanandan, 2002: Experiments in rainfall estimation with a polarimetric radar in a subtropical environment. *J. Appl. Meteor.*, **41,** 674–685.

——, ——, and ——, 2003: An evaluation of a drop distribution–based polarimetric radar rainfall estimator. *J. Appl. Meteor.*, **42,** 652–660.

Bringi, V. N., G.-J. Huang, V. Chandrasekar, and E. Gorgucci, 2002: A methodology for estimating the parameters of a gamma raindrop size distribution model from polarimetric radar data: Application to a squall-line event from the TRMM/Brazil campaign. *J. Atmos. Oceanic Technol.*, **19,** 633–645.

Chandrasekar, V., and V. N. Bringi, 1987: Simulation of radar reflectivity and surface measurements of rainfall. *J. Atmos. Oceanic Technol.*, **4,** 464–478.

Gorgucci, E., V. Chandrasekar, V. N. Bringi, and G. Scarchilli, 2002: Estimation of raindrop size distribution parameters from polarimetric radar measurements. *J. Atmos. Sci.*, **59,** 2373–2384.

Hu, Z., and R. C. Srivastava, 1995: Evolution of raindrop size distribution by coalescence, breakup, and evaporation: Theory and observations. *J. Atmos. Sci.*, **52,** 1761–1783.

Hubbert, J., V. Chandrasekar, V. N. Bringi, and P. Meischner, 1993: Processing and interpretation of coherent dual-polarized radar measurements. *J. Atmos. Oceanic Technol.*, **10,** 155–164.

Huggel, A., W. Schmid, and A. Waldvogel, 1996: Raindrop size distributions and the radar bright band. *J. Appl. Meteor.*, **35,** 1688–1701.

Illingworth, A. J., and T. M. Blackman, 2002: The need to represent raindrop size spectra as normalized gamma distributions for the

interpretation of polarization radar observations. *J. Appl. Meteor.,* **41,** 286–297.

Klaassen, W., 1988: Radar observations and simulation of the melting layer of precipitation. *J. Atmos. Sci.,* **45,** 3741–3753.

Kozu, T., and K. Nakamura, 1991: Rainfall parameter estimation from dual-radar measurements combining reflectivity profile and path-integrated attenuation. *J. Atmos. Oceanic Technol.,* **8,** 259–270.

Kruger, A., and W. F. Krajewski, 2002: Two-dimensional video disdrometer: A description. *J. Atmos. Oceanic Technol.,* **19,** 602–617.

Ryzhkov, A. V., and D. S. Zrnić, 1996: Assessment of rainfall measurement that uses specific differential phase. *J. Appl. Meteor.,* **35,** 2080–2090.

Sauvageot, H., and J. Lacaux, 1995: The shape of averaged drop size distributions. *J. Atmos. Sci.,* **52,** 1070–1083.

Seliga, T. A., and V. N. Bringi, 1976: Potential use of radar differential reflectivity measurements at orthogonal polarizations for measuring precipitation. *J. Appl. Meteor.,* **15,** 69–76.

——, and ——, 1978: Differential reflectivity and differential phase shift: Applications in radar meteorology. *Radio Sci.,* **13,** 271–275.

Tokay, A., A. Kruger, and W. Krajewski, 2001: Comparison of drop size distribution measurements by impact and optical disdrometers. *J. Appl. Meteor.,* **40,** 2083–2097.

Ulbrich, C. W., 1983: Natural variations in the analytical form of the raindrop size distribution. *J. Climate Appl. Meteor.,* **22,** 1764–1775.

Vivekanandan, J., G. Zhang, S. M. Ellis, D. Rajopadhyaya, and S. K. Avery, 2003: Radar reflectivity calibration using differential propagation phase measurement. *Radio Sci.,* **38**, 8049, doi: 10.1029/2002RS002676.

Zhang, G., J. Vivekanandan, and E. Brandes, 2001: A method for estimating rain rate and drop size distribution from polarimetric radar measurements. *IEEE Trans. Geosci. Remote Sens.,* **39,** 830–841.

——, ——, and ——, 2003: The shape–slope relation in gamma raindrop size distributions: Statistical error or useful information? *J. Atmos. Oceanic Technol.,* **20,** 1106–1119.